

Received July 21, 2017, accepted August 1, 2017, date of publication August 21, 2017, date of current version September 6, 2017.

Digital Object Identifier 10.1109/ACCESS.2017.2736558

## INVITED PAPER

# Cerebral Micro-Bleed Detection Based on the Convolution Neural Network With Rank Based Average Pooling

**SHUIHUA WANG<sup>1</sup>, YONGYAN JIANG<sup>2</sup>, XIAOXIA HOU<sup>3</sup>, HONG CHENG<sup>3</sup>, AND SIDAN DU<sup>1</sup>**

<sup>1</sup>School of Electronic Engineering, Nanjing University, Nanjing 210046, China

<sup>2</sup>College of Science, Zhongyuan University of Technology, Zhengzhou 450007, China

<sup>3</sup>Department of Neurology, First Affiliated Hospital of Nanjing Medical University, Nanjing 210029, China

Corresponding author: Shuihua Wang (shuihuawang@ieee.org)

This work was supported by the Program of Natural Science Research of Jiangsu Higher Education Institutions under Grant 16KJB250025.

**ABSTRACT** Cerebral micro-bleed (CMB) is small perivascular hemosiderin deposits from leakage through cerebral small vessels. They can result from cerebra-vascular disease, dementia, or simply from normal aging. It can be visualized via the susceptibility weighted imaging (SWI). Based on the SWI, we propose to use different structures of the CNN with rank-based average pooling to detect the CMB, and compare this method used in this paper to the current state-of-the-art methods. We can find that the CNN with five layers obtains the best performance, with a sensitivity of 96.94%, a specificity of 97.18%, and an accuracy of 97.18%.

**INDEX TERMS** Convolutional neural network, cerebral micro-bleed, network structure, rank based average pooling.

## I. INTRODUCTION

Cerebral micro-bleed (CMB) are small perivascular hemosiderin deposits caused leaked through cerebral small vessels. They can result from Cerebra-vascular disease, dementia or simply from normal aging.

The presence of CMBs can cause hemorrhage-prone pathological disease. Research shows that the intra-cerebral hemorrhage (ICH) has strong relationship with the CMBs. Therefore, the early and accurate detection of the cerebral micro-bleed is necessary.

The development of the magnetic resonance imaging (MRI), has improved our capacity to recognize CMBs. However, due to the paramagnetic properties of blood degradation products, CMB can be better visualized via the Susceptibility Weighted Imaging (SWI) than magnetic resonance imaging (MRI). Instead of the traditional T1 or T2 sequence, SWI as a special sequence of the MRI utilizes a fully flow compensated, gradient and long echo pulse sequence to obtain the images. SWI enhances the contrast and detection based on the paramagnetic properties.

Traditionally, Micro-bleed Anatomical Rating Scale is employed to manually classify CMBs into two categories: “Definite” or “Possible”. However, high intra-observer and inter-observer variability places the accuracy of these manual interpretation in question. In visual screening it is easy to miss

small CMBs and to be confused by CMB mimics. Therefore, the need for automatic methods for detecting CMBs is urgent.

As the development of the magnetic resonance imaging (MRI), CMBs have been increasingly recognized entity based on the MRI images. However, due to the paramagnetic properties of blood degradation products, CMB can be better visualized via the susceptibility weighted imaging (SWI) than magnetic resonance imaging (MRI). In stead of the traditional T1 or T2 sequence, SWI as a special sequence of the MRI utilizes a fully flow compensated, gradient and long echo pulse sequence to obtain the images. SWI enhances the contrast and detection based on the paramagnetic properties.

Traditionally, Micro-bleed Anatomical Rating Scale is employed as the stringent rule to for the manual classification of CMBs into two categories: “Definite” or “Possible”. However, considering the high intra-observer and inter-observer variability, the manual interpretation can be biased. Visual screening is easy to miss small CMBs or be confused with the CMB mimic. Therefore, developing automatic methods for the CMBs detection is in urgent.

Recent years of investigation into CMB have seen several notable developments. Advances in Computer Aid (CAD) system based on the MRI have yielded striking improvements in sensitivity. Fazlollahi *et al.* [1] used the multi-scale Laplacian of Gaussian (MLG) technique to detect possible CMB

candidates. Then a cascaded binary random forests (RF) was used to classify into “Possible” and “Definite”. Bian *et al.* [2] proposed a semi-automatic method based on minimum intensity projected SWI MR images. The 2D fast radial symmetry transform was utilized to first detect the putative CMBs. Followed, The 3D region growing was employed to eliminate the falsely identified CMBs. van den Heuvel *et al.* [3] proposed a two-step method including characterization of twelve features based on the dark and spherical nature of CMBs. They utilized a random forest classifier to identify the locations of the CMB candidates. Then they segmented each identified candidate location, followed by an object-based classifier to eliminate the false positive detections of the voxel classifier. Barnes *et al.* [4] proposed a technique to identify hypo-intensities within the image, which relies on a statistical threshold algorithm. Then, true CMBs were distinguished from other marked hypo-intensities via the support vector machine (SVM) supervised learning classifier. Kuijf *et al.* [5] combined the output of the radial symmetry transform on both echoes to identify the potential CMBs. Charidimou *et al.* [6] discussed the radiological detection methods, criteria for defining CMBs and the standardized rating scales. Zhang *et al.* [7] used leaky rectified linear unit (ReLU) and early stopping to detect the CMBs in CADASIL patients.

These methods have greatly improved detection of CMBs. However, some semiautomatic methods still need manual revision in the last step. For example, though Roy’s method achieved the sensitivity of 85.7%, which is better than manual interpretation. The detection accuracy is still low.

Therefore, in this paper, we propose an algorithm based on the convolution Neural Network (CNN) for the CMBs detection.

This paper is organized as follows: Section 2 introduces the materials used in this paper. Section 3 introduces the proposed method for the CMB detection. Section 4 is the experiment. Section 5 is the conclusion.

## II. MATERIALS

This paper presents data from ten patients with cerebral autosomal-dominant arteriopathy with subcortical infarcts and Leukoencephalopathy (CADASIL). The 3D volumetric images were reconstructed via Syngo MR B17 software [8]. The size of each image is of  $364 \times 448 \times 48$ . Fig 1 shows an SWI image of a patient with micro bleeds

Manual detection was carried out by three neuroradiologists with over twenty years of experience Disagreements were resolved by majority vote. The voxels labelled as “possible” and “definite” were considered as CMB voxels, and others were regarded as non-CMB voxels. Lesion were not included in the analysis if: (1) Via tracking the neighboring slice, we can discard the bleed vessels; (2) They were larger than 10 mm. This research was approved by Institutional review board (IRB) of the First Affiliated Hospital of Nanjing Medical University.

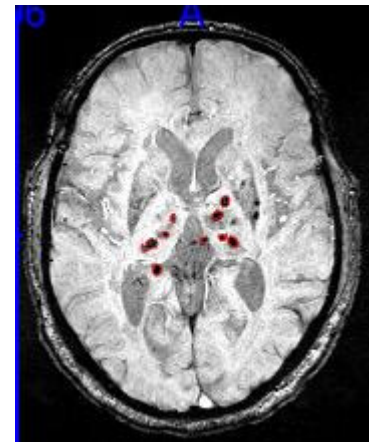


**FIGURE 1.** SWI of a patient with micro-bleeds.

**TABLE 1.** Cost matrix.

		Predicted class	
		CMB	Non-CMB
Actual class	CMB	$C(+, +)$	$C(-, +)$
	Non-CMB	$C(+, -)$	$C(-, -)$

## A. PROCESSING OF DATA IMBALANCE

Considering the data imbalance in our dataset, we employed the cost sensitive learning to improve classification performance. We denote CMB voxels as the positive class (+), which is the minority, and the non-CMB voxels as the majority class (-). Assume  $C(i, j)$  as the cost of predicting the positive example class i to the negative example class j. the cost matrix is displayed in TABLE 1.

If we assume that there is no cost for correct classifications, then the cost ratio can be expressed as:

$$\text{CostRatio} = \frac{C(-, +)}{C(+, -)} \quad (1)$$

Then, the minimum misclassification cost can be expressed as:

$$\text{TotalCost} = C(-, +) \times N_{FN} + C(+, -) \times N_{FP} \quad (2)$$

where  $N_{FN}$  and  $N_{FP}$  stands for the number of the false positive and false negative samples respectively.

## B. IMAGE PREPROCESSING

In order to generate the data samples and target data, a sliding window of size 61 by 61 was applied to the 10 volumetric 3D brain images. Then, the central pixel  $p$  was calculated to generate the target value  $y$ .

$$y = \begin{cases} 1, & \text{Central pixel } p \text{ is CMB} \\ 0, & \text{Central pixel } p \text{ is non-CMB} \end{cases} \quad (3)$$

Meanwhile, each generated sample was constructed as a vector to form the input sample  $x$ .

$$x = V(N(p)) \quad (4)$$

Here,  $N$  means the pixel within the sliding window, and  $V$  stands for the vectorization operation. Then, we can get the input dataset  $X$  and target dataset  $Y$  according to the formulations (3) and (4).

$$\begin{aligned} X &= \{x\} \text{ for all } p \in A \\ Y &= \{y\} \text{ for all } p \in A \end{aligned} \quad (5)$$

in which,  $A$  stands for all the voxels of all subjects' all slices except the border. The 30-pixel borders are ignored as shown in Fig. 2. In order to cover the set  $A$ , the window is set to move from left to the right and from top to down. This resulted in 68,847 CMB voxels and 56,582,536 non-CMB voxels, half of the CMB voxels and half of the non-CMB voxels were used as the training set, and the remaining voxels were used as test set.

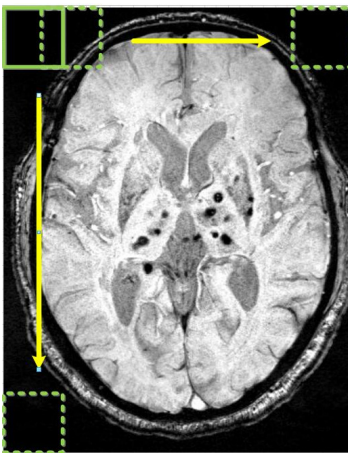


**FIGURE 2.** SNP for sample generating.

### III. CMBS DETECTION BASED ON THE CNN

Recent years, the deep learning shows outstanding performance in object recognition, action recognition, and visual tasks. For example, Li and Yu [8] used the deep CNN [9] to extract the multi-scale features to build the visual saliency model. Milletari *et al.* [10] employed Hough-CNN, which is based on a voting strategy for the segmentation of the deep brain in MRI and ultrasound. Wang *et al.* [11] employed the three-streams for action recognition. Maire *et al.* [12] utilized a convolutional neural network (CNN) to directly predict the pair wise relations that define the affinity matrix, which helps cluster the pixels into regions.

CNN is shift co-variant in detection. Therefore, in this paper, we used CNN for cerebral micro-bleed detection. CNN is composed of multiple layers to implement different functions: Convolution Layer, pooling layer, ReLU layer and fully connected layer. Each layer has learnable parameters and carries out a linear transformation followed by a nonlinear transformation, which is utilized to accelerate the training process. Fig. 3 shows the structure of CNN. Based on the training algorithm, CNN classifies input image sliding as CMB or Non-CMB.

The algorithm is briefly introduced as follows:

#### A. CONVOLUTION LAYER

The operation on two functions of a real valued argument is called convolution. Fig. 4 shows an example of the convolution for the first three steps applied in the spatial domain.

In the convolution layer, a set of linear activation function is generated via convolutions in parallel. Afterwards, there is a nonlinear activation layer to implement a nonlinear transformation, such as the rectified linear activation (ReLU) function.

#### B. ReLU LAYER

The most common functions used to the output of the convolution layer for nonlinear mapping includes hyperbolic tangent activation, softmax activation, rectified linear unit activation etc. For the CNN, we selected the ReLU as the activation function. In mathematic, ReLU can be expressed as follows:

Suppose the inputs to a neuron is  $x$ , then

$$f(x) = \max(0, x) \quad (6)$$

ReLU is first introduced by Hahnloser *et al.* [13] for a dynamic network. For the convolution networks, ReLU is more effective than the logistic sigmoid function, and more practical than the hyperbolic tangent. For these reasons, ReLU has become the most popular activation function for CNN.

#### C. POOLING LAYER

Using all the features obtained from the convolution layer could cause the high burden of the computation for classification. We take an image of size  $61 \times 61$  as an example, and suppose we have learned 400 features over the  $8 \times 8$  inputs. We can get an output of size  $(61 - 8 + 1) \times (61 - 8 + 1) = 2,916$  from the convolution layer. As we had 400 features, this will result in a vector of  $2,916 \times 400 = 1,166,400$  features for a sample. 1+ million features for a classifier could cause the dimension disaster and was easy to be over-fitting. Therefore, pooling is essential for the CNN to reduce the feature numbers.

The pooling function essentially replaces the output of a net with a summary statistic of the nearby outputs at a certain location. The pooling technology can make less sensitive activations in the pooled map than the original feature map to the precise locations of structures within the image.

As it is possible that different pooling functions perform differently, in this paper we used a number of different pooling technologies.

##### 1) MAX POOLING [14]–[16]

In max pooling, the matrix  $u(x, y)$  is applied to the convolution features. The maximum output within a rectangular neighborhood is recorded.

$$M_j = \max_{N \times N} (M_i^{n \times n} u(n, n)) \quad (7)$$

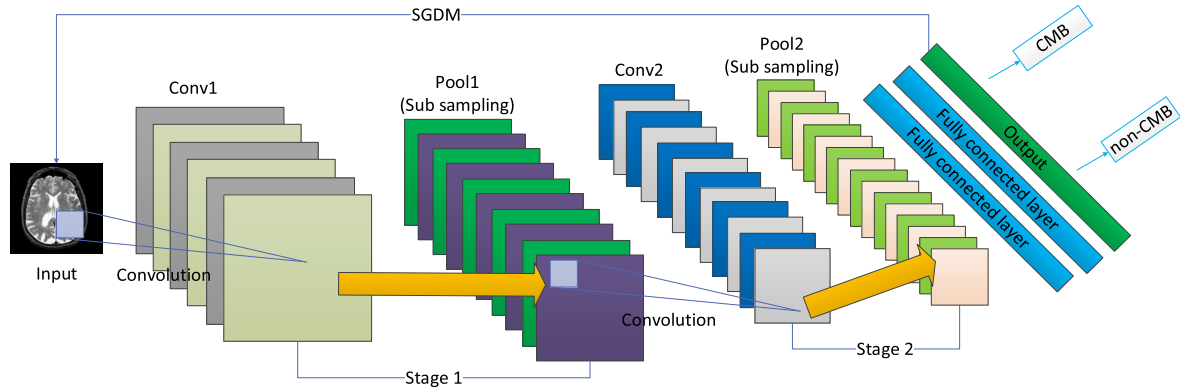


**FIGURE 3.** The Structure of CNN.

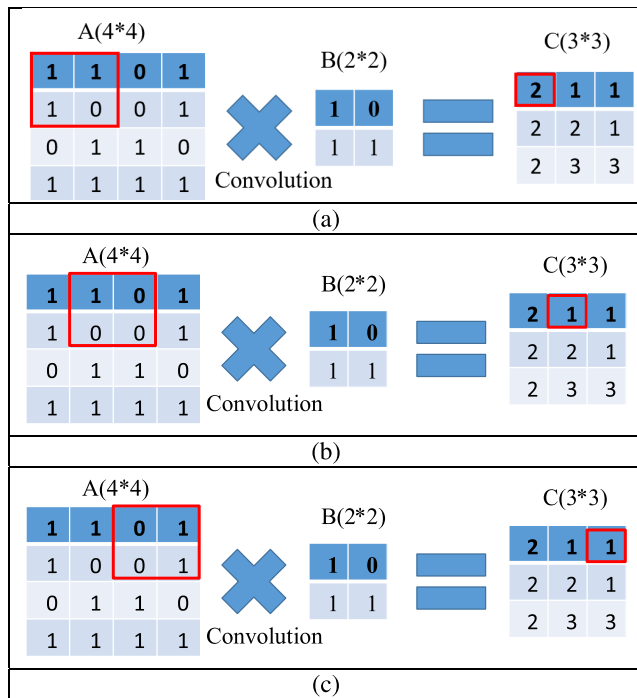


**FIGURE 4.** Sample of Convolution.

Here,  $M$  stands for the inputs of the pooling layer, and  $M_i^{n \times n}$  means a sub-matrix of  $M$ . Fig. 5 shows an example of max pooling.

## 2) AVERAGE POOLING

The average pooling function takes the average over the inputs, multiplies a trainable scalar  $\beta$  and adds a bias  $b$  to get the average outputs within a neighbor window.

$$M_j = \tanh \left( \beta \sum_{N \times N} M_i^{n \times n} + b \right) \quad (8)$$

Both methods obtain a feature map with a lower resolution as shown in Fig. 5.

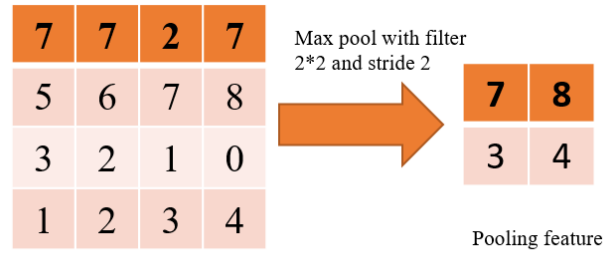


**FIGURE 5.** Sample of Convolution.

## 3) RANK-BASED AVERAGE POOLING (RAP) [17]

Average pooling considers the average operation for the near-zero negative activations in the average pooling may downplay higher activation values, and cause the loss of the discriminative information. Similarly, the non-maximum activations are thrown away fully in the max pooling cause the loss of information. RAP can overcome these problem of the loss of useful information caused by the max pooling and average pooling [18]. The output of the RAP can be expressed as

$$S_j = \frac{1}{t} \sum_{i \in R_j, r_i < t} a_i \quad (9)$$

in which,  $t$  stands for the rank threshold, which determines the types of activations involved in averaging.  $R$  means the pooling region  $j$  in feature maps, and  $t$  represents for the index of each activation within it.  $s_j$  and  $a_i$  stand for the rank of activation  $i$  and the value of activation  $i$  respectively. Here, if  $t = 1$ , it becomes max-pooling. Therefore,  $t$  should be set properly to certain that RAP can get a good trade-off between average pooling and max pooling. Using the median value of  $t$  can remove negative or low value activations while keeping the high response activations.

## D. TRAINING METHOD

The CNN training was implemented on the platform of NVIDIA GeForce GTX 1050 with compute capability of 6.1, clock rate of 1455MHz, and multiprocessors of 5.

**TABLE 2.** Designed structure of CNN.

Layer	Purpose	Filter	No. of filters	Stride	Padding	Weights	Bias	Activation
1	Image input layer							$61 \times 61 \times 1$
2	Convolution+ReLU	$3 \times 3$	40	[3 3]	[1 1]	$3 \times 3 \times 1 \times 40$	$1 \times 1 \times 40$	$21 \times 21 \times 40$
3	Pooling	$3 \times 3$		[1 1]	[1 1]			$21 \times 21 \times 40$
4	Convolution+ReLU	$5 \times 5$	80	[2 2]	[0 0]	$5 \times 5 \times 40 \times 80$	$1 \times 1 \times 80$	$9 \times 9 \times 80$
5	Pooling	$3 \times 3$		[1 1]	[1 1]			$9 \times 9 \times 80$
6	Convolution+ReLU	$3 \times 3$	120	[1 1]	[1 1]	$3 \times 3 \times 80 \times 120$	$1 \times 1 \times 120$	$9 \times 9 \times 120$
7	Pooling	$3 \times 3$		[1 1]	[1 1]			$9 \times 9 \times 120$
8	Convolution+ReLU	$3 \times 3$	160	[1 1]	[1 1]	$3 \times 3 \times 120 \times 160$	$1 \times 1 \times 160$	$9 \times 9 \times 160$
9	Pooling	$3 \times 3$		[1 1]	[1 1]			$9 \times 9 \times 160$
10	Convolution+ReLU	$3 \times 3$	240	[1 1]	[1 1]	$3 \times 3 \times 160 \times 240$	$1 \times 1 \times 240$	$9 \times 9 \times 240$
11	Pooling	$3 \times 3$		[1 1]	[1 1]			$9 \times 9 \times 240$
12	Fully connected layer					$100 \times 19440$	$100 \times 1$	
13	Fully connected layer					$2 \times 100$	$2 \times 1$	

We employed stochastic gradient descent with momentum abbreviated as SGDM, which utilize the full training set to compute the next update of parameters at each iteration. This procedure tends to cover local optima well. Traditionally, it is too slow and intractable on a single machine to compute the cost and gradient for the whole training set in case the dataset is too big to fit in main memory. Furthermore, batch optimization methods do not give an easy way to incorporate new data in an ‘online’ setting. SGD addressed above two problems. Standard gradient descent algorithm update the parameters  $\theta$  of the objective function  $f(\theta)$  as:

$$\theta = \theta - \alpha \nabla_{\theta} E[f(\theta)] \quad (10)$$

in which  $\alpha$  is the learning rate.

However, the standard SGD will tend to oscillate across the narrow ravine in cases the object has the form of a long shallow ravine leading to the optimum and steep walks on the sides. Thus, momentum is adopted for pushing the objective more quickly along the shallow ravine.

The size was set as 128 in our experiments. The initial learning rate was set as 0.01, and was decreased by factor of 10 every 10 epochs. The momentum was set to 0.9. We set the maximum epochs as 30. The loss function was supposed as the Cross entropy.

## IV. EXPERIMENT

### A. NETWORK STRUCTURE

In this paper, we designed the structure of CNN for the cerebral micro-bleed detection. The details are shown in TABLE 2. Here, we designed five layers for the CNN. The pooling method used here is the rank based average pooling. The number of filters used for the convolution is 40, 80, 120, 160, and 240 respectively for each layer.

### B. TRAINING OF CNN

Based on the above designed structure with rank based average pooling, we can get the average classification accuracy of 97.18%. The training accuracy is improved to 90% when the iteration number is  $4 \times 10^6$  as shown in Figure 6. The training loss has a sharp decrease between the iteration number

**TABLE 3.** The confusion matrix of CMB detection for the first run.

		Predicted class	
		CMB(34424)	Non-CMB(28281268)
Actual class	CMB	33632	613704
	Non-CMB	792	27667564

**TABLE 4.** Specificity, sensitivity and accuracy of designed CNN for 10 runs.

Measurements	Sensitivity (%)	Specificity (%)	Accuracy (%)
1 <sup>st</sup> run	97.70	97.83	97.83
2 <sup>nd</sup> run	96.89	96.91	96.91
3 <sup>rd</sup> run	97.58	97.56	97.56
4 <sup>th</sup> run	96.53	96.58	96.58
5 <sup>th</sup> run	97.71	97.75	97.75
6 <sup>th</sup> run	96.83	97.12	97.12
7 <sup>th</sup> run	95.27	96.74	96.74
8 <sup>th</sup> run	95.82	95.93	95.93
9 <sup>th</sup> run	96.85	97.10	97.10
10 <sup>th</sup> run	98.20	98.32	98.32
Std	0.90687	0.70	0.70
Mean	96.94	97.18	97.18

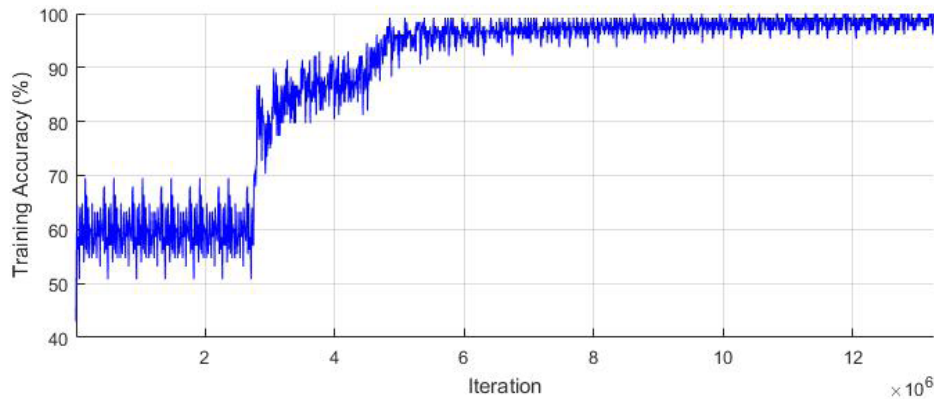
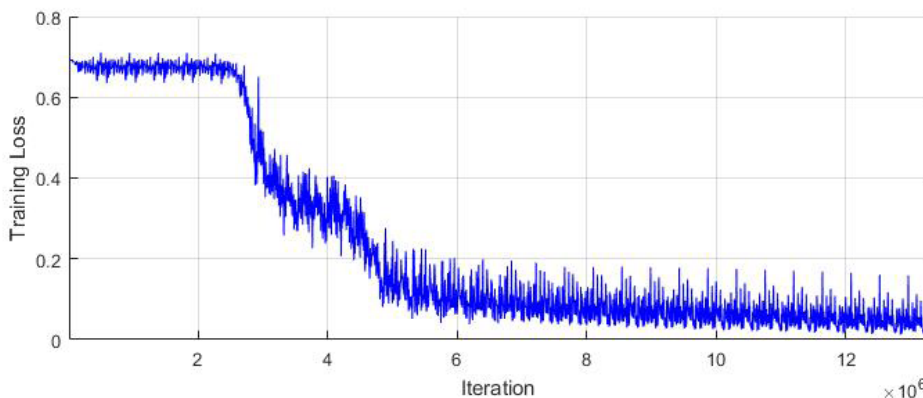
$3 \times 10^6$  and  $6 \times 10^6$  as shown in Figure 7. Then, the decreasing slows down until get the best training loss.

### C. CONFUSION MATRIX

From TABLE 3, we can find that the designed CNN correctly detected 33632 CMB voxels and 27667564 non-CMB voxels on the first run. TABLE 4 shows the result of 10 runs. The average sensitivity across these runs is 96.94%, average specificity as 97.18% and average accuracy as 97.18%. The standard Deviation of the sensitivity, specificity and accuracy based on the 10 run are 0.90687, 0.70 and 0.70 respectively.

### D. COMPARISON OF DIFFERENT STRUCTURES OF CNN

In this paper, we designed a five layer CNN for the CMBs detection. Research shows, the layer number has strong relation with the performance. Therefore, we compare 5-layer CNN with the 3-layer CNN and 9-layer CNN. The result is

**FIGURE 6.** Training accuracy.**FIGURE 7.** Training loss.**TABLE 5.** CNN with different structures.

	Sensitivity (%)	Specificity (%)	Accuracy (%)
CNN (5-Layer)	96.94	97.18	97.18
CNN (3-Layer)	96.83	96.85	96.85
CNN (9-Layer)	96.89	97.53	97.53

shown in TABLE 5, we can find that the 5-layer CNN get the best performance. It achieved the sensitivity of 96.94%, specificity of 97.18% and accuracy of 97.18%.

In this paper, we proposed using CNN for the cerebral micro-bleed classification. For the material, we have ten cerebral autosomal-dominant arteriopathy with subcortical infarcts and Leukoencephalopathy (CADASIL) patients. We first employed the SNP to generate the input images. Considering the data imbalance of the CMB voxels and Non-CMB voxels, Cost ratio is used. Finally, we used CNN for the CMB voxel detection. Sensitivity, Specificity and accuracy are employed as the measurements. The 5-layer CNN achieved the sensitivity as 96.94 %, the specificity as 97.18% and accuracy as 97.18%. Due to the large number of non-CMB voxels, the specificity is nearly approximate the accuracy. However, the main purpose in this research is

**TABLE 6.** Comparison of different pooling technologies.

	Max pooling	Average pooling	RAP (Proposed)
Accuracy	96.83%	97.02%	<b>97.18%</b>

to detect the CMB voxels, Therefore, the sensitivity is more important than the other two measurements. In order to prove the efficiency of the designed structure, we compared CNN with different layers including 3 layer CNN and 9 layer CNN, the results are shown in TABLE 5.

#### E. POOLING METHOD COMPARISON

Based on the above designed 5 layer CNN structures, we compared the different pooling technology including max pooling, average pooling and Rank-based pooling via the average of 10 runs. The results of the different pooling method are shown in TABLE 6.

As we can see from the TABLE 6, the ranked-based average pooling method has better performance than max pooling and average pooling. This is because the RAP kept the higher activation values that are thrown out by the average operation in the average pooling and the non-maximum activations, which are thrown out by max pooling.

**TABLE 7. Comparison of the State-of-the art-approaches.**

Method	Sensitivity (%)	Specificity (%)	Accuracy (%)
MRST + RF [19]	85.7	99.5	
SNP+SLFN+LReLU [20]	93.05	93.06	93.06
7-layer SAE [21]	95.13±0.84	93.33±0.84	94.23±0.84
WE + NBC [22]	76.90±1.81	76.91±1.58	76.90±1.67
Proposed CNN (5-layer)	96.94	97.18	97.18

## F. COMPARISON TO STATE-OF-THE-ART APPROACHES

In order to prove the efficiency of the designed structure for the cerebral micro-bleed detection, we compare CNN to the current state-of-the art approaches. MRST+RF stands for multiple radial symmetry transforms (MRST) and random forest, which is proposed by Roy *et al.* [19] for the CMB segmentation. SNP+SLFN+LReLU [7] stands for the sliding neighborhood processing, single layer forward neural network and leaky rectified linear unit. SAE [20] means sparse auto-encoder. WE + NBC [21] means the wavelet entropy and naïve Bayes classifier. Meanwhile, we designed multiple layer of the CNN, we can find that the CNN has better performance than the above existed method. For the multiple layers, the 5-layer CNN has the best performance.

The result of comparison is shown in TABLE 7. The performance of 5-layer CNN was superior to the other four methods.

## V. CONCLUSION

In this paper, we proposed to use CNN for the CMB detection. The result is shown in TABLE 4

In order to prove the efficiency of the proposed structure of CNN, we compared CNN with multiple layer, and CNN with different pooling methods. The results are shown in TABLE 5 and TABLE 6. Meanwhile, we compared our proposed method with the current state of art methods as shown in TABLE 7. In summary, we can find that the CNN with 5 layer structure and rank based pooling method obtained the best performance of all the methods tested.

Our future work will focus on collecting more data to test the performance of CNN, designing the optimal CNN, including the number of layers, and the parameters of each layer.

## REFERENCES

- [1] A. Fazlollahi *et al.*, “Computer-aided detection of cerebral microbleeds in susceptibility-weighted imaging,” *Comput. Med. Imag. Graph.*, vol. 46, pp. 269–276, Dec. 2015.
- [2] W. Bian, C. P. Hess, S. M. Chang, S. J. Nelson, and J. M. Lupo, “Computer-aided detection of radiation-induced cerebral microbleeds on susceptibility-weighted MR images,” *NeuroImage, Clin.*, vol. 2, pp. 282–290, Dec. 2013.
- [3] T. L. A. van den Heuvel *et al.*, “Automated detection of cerebral microbleeds in patients with traumatic brain injury,” *NeuroImage, Clin.*, vol. 12, pp. 241–251, Feb. 2016.
- [4] S. R. S. Barnes, “Semiautomated detection of cerebral microbleeds in magnetic resonance images,” *Magn. Reson. Imag.*, vol. 29, no. 6, pp. 844–852, Jul. 2011.
- [5] H. J. Kuijf *et al.*, “Efficient detection of cerebral microbleeds on 7.0 T MR images using the radial symmetry transform,” *NeuroImage*, vol. 59, no. 3, pp. 2266–2273, 2012.
- [6] A. Charidimou, H. R. Jäger, D. J. Werring, “Cerebral microbleed detection and mapping: Principles, methodological aspects and rationale in vascular dementia,” *Experim. Gerontol.*, vol. 47, no. 11, pp. 843–852, 2012.
- [7] Y. D. Zhang *et al.*, “Voxelwise detection of cerebral microbleed in 398 CADASIL patients by leaky rectified linear unit and early stopping,” *Multimedia Tools Appl.*, pp. 1–21, Jan. 2017. [Online]. Available: <https://link.springer.com/article/10.1007/s11042-017-4383-9>
- [8] G. Li and Y. Yu, “Visual saliency detection based on multiscale deep CNN features,” *IEEE Trans. Image Process.*, vol. 25, no. 11, pp. 5012–5024, Nov. 2016.
- [9] Y. LeCun, L. Bottou, Y. Bengio, and P. Haffner, “Gradient-based learning applied to document recognition,” *Proc. IEEE*, vol. 86, no. 11, pp. 2278–2324, Nov. 1998.
- [10] F. Milletari *et al.*, “Hough-CNN: Deep learning for segmentation of deep 407 brain regions in MRI and ultrasound,” *Comput. Vis. Image Understand.*, 2017. [Online]. Available: <https://doi.org/10.1016/j.cviu.2017.04.002>
- [11] L. Wang, “Three-stream CNNs for action recognition,” *Pattern Recognit. Lett.*, vol. 92, pp. 33–40, Jun. 2017.
- [12] M. Maire, T. Narihira, and S. X. Yu, “Affinity CNN: Learning pixel-centric pairwise relations for figure/ground embedding,” in *Proc. IEEE Conf. Comput. Vis. Pattern Recognit. (CVPR)*, Jun. 2016, pp. 174–182.
- [13] R. H. R. Hahnloser, R. Sarpeshkar, M. A. Mahowald, R. J. Douglas, and H. S. Seung, “Correction: Digital selection and analogue amplification coexist in a cortex-inspired silicon circuit,” *Nature*, vol. 408, p. 1012, Dec. 2000.
- [14] J. Masci, A. Giusti, D. Ciresan, G. Fricout, and J. Schmidhuber, “A fast learning algorithm for image segmentation with max-pooling convolutional networks,” in *Proc. IEEE Int. Conf. Image Process.*, Sep. 2014, pp. 2713–2717.
- [15] A. Giusti, D. C. Ciresan, J. Masci, L. M. Gambardella, and J. Schmidhuber, “Fast image scanning with deep max-pooling convolutional neural networks,” in *Proc. IEEE Int. Conf. Image Process.*, Sep. 2014, pp. 4034–4038.
- [16] D. C. Ciresan, A. Giusti, L. M. Gambardella, and J. Schmidhuber, “Mitosis detection in breast cancer histology images with deep neural networks,” *Proc. Int. Conf. Med. Image Comput. Comput.-Assist. Intervention*, vol. 16, 2013, pp. 411–418.
- [17] B. Fernando *et al.*, “Rank pooling for action recognition,” *IEEE Trans. Pattern Anal. Mach. Intell.*, vol. 39, no. 4, pp. 773–787, 2017.
- [18] Z. Shi, Y. Wu, and Y. Ye, “Rank-based pooling for deep convolutional neural networks,” *Neural Netw.*, vol. 83, pp. 21–31, Nov. 2016.
- [19] A. Giusti, D. C. Ciresan, J. Masci, L. M. Gambardella, and J. Schmidhuber, “Fast image scanning with deep max-pooling convolutional neural networks,” in *Proc. IEEE Int. Conf. Image Process.*, Melbourne, VIC, Australia, 2013, pp. 4034–4038, doi: 10.1109/ICIP.2013.6738831.
- [20] H. Chen, “Seven-layer deep neural network based on sparse autoencoder for voxelwise detection of cerebral microbleed,” *Multimedia Tools Appl.*, vol. 5, pp. 1–18, 2017, doi: 10.1007/s11042-017-4554-8.
- [21] B. Gagnon, “Cerebral microbleed detection by wavelet entropy and naive Bayes classifier,” in *Proc. 2nd Int. Conf. Biomed. Biol. Eng. (BBE)*, 2017, pp. 321–325.



**SHUIHUA WANG** was born in Qidong, Jiangsu, China, in 1985. She received the B.S. degree from Southeast University in 2008, the M.S. degree from The City University of New York in 2012, and the Ph.D. degree from Nanjing University in 2017.

She is currently an Assistant Professor with Nanjing Normal University.



**YONGYAN JIANG** was born in Jilin, Meihekou, in 1978. She received the degree in applied mathematics from the Harbin Institute of Technology. She is currently a Lecturer at Zhongyuan University. She is mainly involved in the application of differential equations and information processing.



**HONG CHENG** is currently a Chief Physician, an Associate Professor, and a Master Tutor with the First Affiliated Hospital of Nanjing Medical University. She have devoted herself in neurology for over 20 years in Jiangsu Province Hospital. She published over 30 papers. She took participate in nearly five NSFC and provincial grants.



**XIAOXIA HOU** is currently pursuing the master's degree in neurology with Nanjing Medical University. She is also receiving clinical training with Jiangsu Province Hospital.



**SIDAN DU** received the Ph.D. degree in physics from Nanjing University, Nanjing, China, in 1997. She is currently a Professor with the School of Electronic Science and Engineering, Nanjing University. Her research interests include in digital imaging processing and computer vision.

• • •